Article

Discovery Medicine 2026; 38(204): 199–214
https://doi.org/10.24976/Discov.Med.202638204.16

Research on the Role and Mechanism of MCM10 in Colorectal Cancer Based on Bioinformatics Analysis and Experimental Validation

Chuang Zhang[1], Shao-Ke Wang[1], Chen-Feng Yu[1], Yan-Long Liu[1,*], Bin-Bin Cui[1,*]

[1]Department of Colorectal Surgery, Harbin Medical University Cancer Hospital, 150081 Harbin, Heilongjiang, China
*Correspondence: liuyanlong@hrbmu.edu.cn (Yan-Long Liu); binbincui@hrbmu.edu.cn (Bin-Bin Cui)
Submitted: 20 October 2025 Revised: 28 November 2025 Accepted: 17 December 2025 Published: 20 January 2026

Background: This study systematically evaluated the expression profile and functional significance of *minichromosome maintenance 10* (*MCM10*) in colorectal cancer (CRC), assessed its association with the tumor immune microenvironment, and investigated its role in regulating cellular proliferation, migration, invasion, and stemness, thereby highlighting its potential as a therapeutic candidate.

Methods: Transcriptomic datasets were accessed from publicly available databases (GEO and TCGA). The data were analyzed to determine *MCM10* expression and assess its association with immune cell infiltration. Functional enrichment profiling and molecular network modeling were performed to uncover underlying mechanisms. Furthermore, *in vitro* validation, including quantitative real-time polymerase chain reaction (qRT-PCR), Western blot analysis, 3-(4,5-dimethylthiazol-2-yl)-2,5-diphenyltetrazolium bromide (MTT) proliferation assays, Transwell migration and invasion assays, and tumor sphere formation assays, was conducted to determine the biological effects of MCM10 on CRC cells.

Results: *MCM10* was upregulated in CRC tissues and demonstrated a positive association with immune-cell infiltration, particularly helper T cells and T helper 2 (Th2) cells. Notably, *MCM10* expression was substantially higher in CRC tissues compared with adjacent normal tissues ($p < 0.001$), consistent with TCGA and GTEx cohort analyses. Furthermore, *MCM10* was enriched in cancer-related signaling pathways and immune regulatory processes. Functional assays demonstrated that *MCM10* overexpression promoted CRC cell proliferation, migration, invasion, and stemness, while its knockdown produced the opposite effects.

Conclusion: Our findings confirm a pivotal role of *MCM10* in CRC, suggesting its potential as a diagnostic biomarker and therapeutic target. The findings offer promising insights into the molecular biology of CRC and provide a foundation for the development of precision treatment strategies.

Keywords: colorectal cancer; MCM10; tertiary lymphoid structure; immune infiltration

Introduction

Colorectal cancer (CRC) is a frequently diagnosed malignant tumor worldwide, with approximately 2 million new cases reported in 2020 [1]. Multiple variables contribute to its development and progression, including age, gender, genetic predisposition, increased body mass, and smoking [2]. Current treatment for CRC includes endoscopic interventions, surgical resection, radiation therapy, chemotherapy, targeted therapies, and immunotherapy. For metastatic CRC, regimens that combine a targeted agent are recommended [3,4]. Despite advances in diagnosis and therapy, CRC-associated morbidity and mortality remain significantly high, and the prognostic outcomes for metastatic disease are still suboptimal, with a median overall survival time of about 25–30 months and a five-year survival rate below 20% [4,5]. Therefore, exploring the biological features of distinct CRC subsets may help identify predictive biomarkers for diagnosis and prognosis and guide more individualized treatment approaches.

T and B cells play critical roles in adaptive immune responses and have been linked to improved prognosis in patients with CRC [6–8]. Mature tertiary lymphoid structures (TLSs) are characterized by organized T-cell and B-cell zones and represent ectopic lymphoid organs that help sustain immune response at sites of chronic inflammation [9]. TLSs have been identified across multiple cancer types, with context-dependent effects [10]; however, tumor-related TLSs are generally linked to a favorable prognosis [11]. In CRC, both the distribution and density of TLSs have been associated with molecular subtypes and survival in metastatic cases [12], suggesting their potential relevance to anti-CRC therapeutic approaches. Furthermore, experimental evidence demonstrated that Helicobacter hepaticus-induced T follicular helper cells can promote TLS formation and inhibit CRC growth [13]. Currently, ro-

bust identification and quantification of TLS are challenging, but transcriptomic approaches provide an opportunity to derive TLS-associated gene signatures for more comprehensive evaluation [14]. Therefore, investigating TLS-related gene signatures may improve prognostic prediction in CRC.

Minichromosome maintenance proteins (MCMs) are a family of highly conserved proteins that are crucial for initiating eukaryotic genome replication and may also affect cell-cycle regulation and cellular proliferation [15,16]. Studies have indicated that MCMs are valuable for diagnosis and prognostic prediction across different malignancies [17–19]. *MCM10*, a member of this family, plays an essential role in DNA replication, and its dysregulation can lead to genomic instability and carcinogenesis [20]. Aberrant *MCM10* expression has been reported in several pathological conditions, including various malignancies, and supports its potential as a prognostic biomarker [16,18]. In CRC specifically, *MCM10* has been reported to be upregulated and has been proposed as a signature gene [21]. However, the explicit role of *MCM10* in CRC remains to be elucidated.

In this study, we systematically assessed the expression patterns and functional relevance of *MCM10* in CRC using an integrated approach combining bioinformatics analyses with *in vitro* experiments. Using publicly available transcriptomic datasets, we analyzed the correlation between *MCM10* expression and the CRC immune milieu and explored potential underlying molecular mechanisms through functional enrichment analyses and molecular network construction. Furthermore, we validated these findings experimentally by evaluating how *MCM10* affects cancer cell proliferation, migration, invasion, and stemness *in vitro*. The findings provide multi-dimensional evidence supporting *MCM10*'s role in CRC biology, enhance understanding of molecular mechanisms underlying CRC development and progression, and indicate *MCM10* as a potential candidate for precision diagnosis, biomarker development, and personalized therapeutic approaches.

Materials and Methods

Data Source and Expression Analysis

Three CRC datasets (GSE22598, GSE32323, and GSE110224) were retrieved from the GEO repository. The gene expression arrays in these 3 datasets were generated using the Affymetrix GPL570 (U133_Plus_2) microarray platform. The datasets were merged using the inSilicoMerging R package (version 1.24.0), and batch effects were removed using the method described by Johnson WE *et al*. [22]. Batch correction was conducted using the empirical Bayes–based ComBat algorithm implemented in the sva R package (version 3.44.0). The impact of batch adjustment was assessed using boxplots, density plots, and uniform manifold approximation and projection (UMAP) visualizations generated with the ggplot2 R package, comparing distribution pre- and post-correction. The differentially expressed genes (DEGs) between CRC and control samples were determined using the limma package (version 3.52.2) in R (version 4.2.1; R Foundation for Statistical Computing, Vienna, Austria), applying thresholds of $|\log_2 FC| > 1$ and adjusted $p < 0.05$.

Immune Cell Infiltration in CRC Patients

The immune infiltration pattern in the tumor microenvironment (TME) of CRC patients was assessed with the Microenvironment Cell Populations-counter (MCPcounter) algorithm using the MCPcounter package (version 1.2.0) [23]. MCPcounter quantifies the relative abundance of immune-cell landscape across samples based on representative marker genes. Ten different immune cell types were quantified, including B lineage, cytotoxic lymphocytes ($CD8^+$ and related T-cell subsets), NK cells, monocyte-derived populations, myeloid DCs, endothelial cells, fibroblasts, and neutrophils, as well as overall T cell signals. The abundance of these immune cell populations was compared between colorectal carcinoma tissues and surrounding non-tumor colorectal tissues. Results were presented as a heatmap using the R pheatmap package (version 1.0.12). Furthermore, the expression levels of TLS signature genes, Tfh-associated genes, TLS chemokines, and Th1/B cell signature genes were compared between CRC and adjacent normal samples and displayed using boxplots.

MCM10 Expression and Correlation With CRC Immunity

Using RNA-seq data from the TCGA-COAD and TCGA-READ projects along with normal tissue data from the GTEx database, MCM10 expression was compared in both paired and unpaired samples and visualized accordingly. Pan-cancer expression levels of MCM10 across diverse tumor types were evaluated using TCGA data and visualized as boxplots. Immunohistochemical staining results for MCM10 in CRC and normal tissues were sourced from The Human Protein Atlas (HPA) database (https://www.proteinatlas.org/). Associations between MCM10 levels and immune-cell infiltration in CRC were evaluated using single-sample gene set enrichment analysis (ssGSEA) implemented in the GSVA R package (version 1.44.5). Relationships between MCM10 levels and clinicopathologic features of CRC patients were assessed and outlined in Table 1. Finally, the diagnostic performance of MCM10 to differentiate between CRC tissues and adjacent normal tissues was evaluated using the receiver operating characteristic (ROC) curve analysis in the pROC package (version 1.18.0).

Single-Gene Differential Analysis of MCM10 in CRC

Using RNA-seq data from the TCGA-COAD and TCGA-READ cohorts, single-gene differential analysis for

Table 1. Correlation between MCM10 expression and the clinicopathologic features of CRC patients.

Characteristic	Low expression of MCM10	High expression of MCM10	*p*-value
n	54	77	
Pathological T stage, n (%)			0.564
T1 & T2	11 (8.4%)	19 (14.5%)	
T3 & T4	43 (32.8%)	58 (44.3%)	
Pathological N stage, n (%)			0.037
N0	23 (17.6%)	47 (35.9%)	
N1 & N2	31 (23.7%)	30 (22.9%)	
Pathological M stage, n (%)			0.192
M0	45 (34.4%)	70 (53.4%)	
M1	9 (6.9%)	7 (5.3%)	
Pathological stage, n (%)			0.037
Stage I & Stage II	23 (17.6%)	47 (35.9%)	
Stage III & Stage IV	31 (23.7%)	30 (22.9%)	
BMI, n (%)			0.232
$\leq$25	13 (9.9%)	26 (19.8%)	
>25	41 (31.3%)	51 (38.9%)	
Histological type, n (%)			1.000
Adenocarcinoma	49 (37.4%)	71 (54.2%)	
Mucinous adenocarcinoma	5 (3.8%)	6 (4.6%)	
Residual tumor, n (%)			0.639
R0	54 (41.2%)	75 (57.3%)	
R1 & R2	0 (0%)	2 (1.5%)	
Perineural invasion, n (%)			0.422
No	38 (29%)	59 (45%)	
Yes	16 (12.2%)	18 (13.7%)	
Lymphatic invasion, n (%)			0.152
No	36 (27.5%)	60 (45.8%)	
Yes	18 (13.7%)	17 (13%)	
History of colon polyps, n (%)			<0.001
No	40 (30.5%)	73 (55.7%)	
Yes	14 (10.7%)	4 (3.1%)	
Colon polyps present, n (%)			0.152
No	36 (27.5%)	60 (45.8%)	
Yes	18 (13.7%)	17 (13%)	
Neoplasm type, n (%)			0.464
Colon adenocarcinoma	41 (31.3%)	54 (41.2%)	
Rectum adenocarcinoma	13 (9.9%)	23 (17.6%)	
OS event, n (%)			0.311
Alive	46 (35.1%)	70 (53.4%)	
Dead	8 (6.1%)	7 (5.3%)	

MCM10, minichromosome maintenance 10; CRC, colorectal cancer.

MCM10 in CRC was conducted using the DESeq2 R package (version 1.34.0) implemented in R software (version 4.2.1; R Foundation for Statistical Computing, Vienna, Austria). CRC samples were then stratified into the high- or low-MCM10 expression groups. The DEGs between these two groups were determined using thresholds of $|\log_2 FC| > 1$ and adjusted $p < 0.05$. The resulting DEGs were subjected to Gene Ontology (GO) and Kyoto Encyclopedia of Genes and Genomes (KEGG) enrichment analyses using the clusterProfiler R package (version 4.6.0), and the results were visualized with the ggplot2 R package (version 3.4.0), as bubble plots or bar plots. Additionally, gene set enrichment analysis (GSEA) was performed using the clusterProfiler R package (version 4.6.0), and the results were visualized with the enrichplot (version 1.18.0) and ggridges (version 0.5.4) R packages.

Identification of Molecular Subtypes and Correlation With Gene Mutation

Differential expression of TLS signature genes in CRC and adjacent normal tissues was analyzed using the limma R package (version 3.52.2) and visualized as a heatmap. CRC patients were then stratified into TLS-positive and TLS-negative subgroups using the ConsensusClusterPlus R package (version 1.60.0) based on the expression of TLS signature genes [24]. The optimal number of clusters was set to two, guided by the consensus distribution function and the delta-area plot.

Gene annotation files (gff3, v22, and v23) were retrieved from the GENCODE database (https://www.gencodegenes.org/human/). DEGs between Cluster 1 (C1, TLS-positive) and Cluster 2 (C2, TLS-negative) were identified using thresholds of $|\log_2 FC| > 1$ and adjusted $p < 0.05$, followed by GO and KEGG enrichment analyses. For genomic variation analyses, mutation types and mutation burdens were compared between C1 and C2. Somatic mutational data in mutation annotation format were acquired from Genomic Data Commons. Analyses assessed non-synonymous variants, including nonsense, missense, frameshift, splice-site, and in-frame mutations, to evaluate their relationships with immune signatures. Finally, significantly mutated genes were identified using the MutSigCV algorithm (version 1.41), developed by the Broad Institute (Cambridge, MA, USA).

Experimental Validation

Cell Culture and Grouping

This study employed fetal human colonic epithelial cells (FHC) and two CRC cell lines (HCT116 and SW480) to investigate the role of MCM10 in CRC. FHC (CRL-1831) and HCT116 (CCL-247) cells were obtained from ATCC, and SW480 (GDC0143) cells were purchased from CCTCC. All cell lines were authenticated by short tandem repeat (STR) profiling prior to use, and the results were confirmed to be consistent with the reference profiles provided by the corresponding cell banks. All cell lines were cultured in RPMI-1640 medium containing 10% fetal bovine serum and incubated at 37 °C in a humidified incubator with 5% CO_2. Mycoplasma testing was conducted before experiments, and only mycoplasma-free cultures were used in subsequent analyses.

The baseline groups included FHC, HCT116, and SW480 cells. For HCT116 cells, additional transfection groups were established to modulate *MCM10* expression: a sh-NC group (HCT116 cells transfected with control shRNA), a sh-MCM10 group (cells transfected with MCM10-interfering shRNA), an oe-NC group (cells transfected with the negative control pcDNA3.1 plasmid), and an oe-MCM10 group (cells transfected with the MCM10 overexpression plasmid pcDNA3.1-MCM10). The pcDNA3.1-MCM10 overexpression plasmid and the corresponding pcDNA3.1 empty vector (oe-NC) were constructed by a commercial biotechnology company (Yujia Biotechnology, Guangzhou, China).

For *MCM10* knockdown, a short hairpin RNA targeting human *MCM10* (sh-MCM10, targeting sequence: 5′-GGAGAAACAGGAGAGACAAGA-3′) and a non-targeting control shRNA (sh-NC, targeting sequence: 5′-CAACAAGATGAAGAGCACCAA-3′) were used. The sh-NC plasmid was the MISSION® pLKO.1-puro Non-Mammalian shRNA Control (Sigma-Aldrich, SHC002), which does not target any known mammalian gene.

Quantitative Real-Time Polymerase Chain Reaction (qRT-PCR)

Total RNA was isolated from cells in each group (FHC, HCT116, SW480, sh-NC, sh-MCM10, oe-NC, and oe-MCM10) using Trizol reagent (Thermo Fisher Scientific, Waltham, MA, USA, Cat. No. 15596026). RNA purity was determined by ensuring an A260/A280 ratio of 1.8–2.0. Subsequently, 1 µg of total RNA was converted into cDNA using a commercial reverse transcription kit. qRT-PCR was then performed with MCM10-specific primers (Table 2) using SYBR Green chemistry (Thermo Fisher Scientific, Waltham, MA, USA, Cat. No. 4402959) on a QuantStudio™ 5 Real-Time PCR system (Thermo Fisher Scientific, Waltham, MA, USA, Cat. No. A28140). The thermocycler conditions included an initial denaturation at 95 °C for 3 minutes, followed by 40 amplification cycles of 95 °C for 15 seconds and 60 °C for 30 seconds. A melting-curve analysis was performed to verify amplification specificity. Relative gene expression was quantified using the $2^{-\Delta\Delta Ct}$ approach: ΔCt values were obtained by normalizing the target gene to the reference gene, and $\Delta\Delta$Ct values were calculated by comparing experimental groups with the corresponding controls.

Western Blotting

Western blotting was conducted to determine protein expression levels. Cells were lysed in RIPA lysis and extraction buffer (Thermo Fisher Scientific, Waltham, MA, USA, Cat. No. 89900), and total protein concentrations were quantified using the bicinchoninic acid (BCA) assay (Thermo Fisher Scientific, Waltham, MA, USA, Cat. No. 23225). Equal amounts of protein (30 µg per lane) were resolved on SDS-PAGE and subsequently transferred onto PVDF membranes (IPVH00010, Millipore, Billerica, MA, USA). After blocking with 5% skim milk for one hour at room temperature, membranes were incubated overnight at 4 °C with primary antibodies against MCM10 (1:1000, Abcam, ab3733, Cambridge, UK), SOX2 (1:1500, Abcam, ab97959, Cambridge, UK), Oct4 (1:1000, Abcam, ab181557, Cambridge, UK), NANOG (1:1000, Abcam, ab109250, Cambridge, UK), KLF4 (1:1000, Abcam, ab215036, Cambridge, UK), and β-actin (1:5000, Abcam, ab8227, Cambridge, UK). The following day, membranes were incubated for 1 hour at room temperature with

Table 2. Primers used in this study.

Name	Forward primer (5′-3′)	Reverse primer (5′-3′)
MCM10	CCGGCATCGGCCAAGAT	GGCTGACTCATTTTCTTCCAGC
GAPDH	AAGATCATCAGCAATGCCTCC	AGGTTTTTCTAGACGGCAGG

MCM10, minichromosome maintenance 10; GAPDH, glyceraldehyde-3-phosphate dehydrogenase.

an HRP-conjugated goat anti-rabbit IgG secondary antibody (1:5000, Abcam, ab205718, Cambridge, UK). Protein bands were visualized using a ChemiDoc™ MP Imaging System (Bio-Rad, Hercules, CA, USA) and quantified using ImageJ software (Version 1.53, NIH, Bethesda, MD, USA).

3-(4,5-Dimethylthiazol-2-yl)-2,5-Diphenyltetrazolium Bromide (MTT) Assay

Cell proliferation was assessed using the MTT assay. Cells from each group were seeded into 96-well plates at a density of 1×10^4 cells per well and incubated for 24, 48, or 72 hours. At each time point, 20 µL of MTT reagent (5 mg/mL; Sigma-Aldrich, St. Louis, MO, USA; Cat. No. M5655) was added, followed by a 4-hour incubation at 37 °C in 5% CO_2 to allow formazan crystal formation. The supernatant was then removed, and 150 µL of DMSO (DMSO; Sigma-Aldrich, St. Louis, MO, USA; Cat. No. D2650) was added to solubilize the crystals. Culture plates were gently agitated for 10 minutes at 37 °C, and absorbance was recorded at 570 nm using a microplate reader (Model 680, Bio-Rad, Hercules, CA, USA). All measurements were conducted within the linear detection range specified by the manufacturer. Cell viability was expressed as a percentage of the absorbance relative to the corresponding control group (sh-NC or oe-NC).

Transwell Assay

Transwell assays were conducted using chambers fitted with 8-µm pore inserts. For migration assays, inserts were used without coating, while for invasion assays, the inserts were precoated with Matrigel (BD Biosciences, San Jose, CA, USA; Cat. No. 356234), which was allowed to polymerize at 37 °C for 30 minutes. Cells in the logarithmic growth phase were collected, resuspended in serum-free medium, and adjusted to a final density of 5×10^4 cells/mL. A 200 µL of the cell suspension was added to the upper chamber, and 600 µL of medium supplemented with 10% FBS was added to the lower chamber as a chemoattractant. The chambers were incubated for 24 hours (migration) or 48 hours (invasion).

Following incubation, inserts were washed twice with PBS, fixed with 4% paraformaldehyde for 15 minutes, and subsequently stained with crystal violet (Sigma-Aldrich, St. Louis, MO, USA; Cat. No. C0775) for 10 minutes. Non-migrated/non-invaded cells on the upper surface of the membrane were removed gently with a cotton swab, leaving cells that had migrated or invaded for analysis. Migrated or invaded cells were enumerated using an Olympus IX73 microscope (Olympus Corporation, Tokyo, Japan) in five randomly selected fields per insert. To ensure reliability and comparability, Matrigel coating and cell seeding were kept uniform across groups. Cell counting was performed independently by two investigators in a blinded manner to minimize subjective bias.

Sphere Formation Assay

The tumorsphere formation assay was used to evaluate the stemness of colorectal cancer cells and to examine the regulatory effect of MCM10 on cellular stemness. FHC and HCT116 cells from the sh-NC, sh-MCM10, oe-NC, and oe-MCM10 groups were used in this assay. Following trypsinization, a single-cell suspension was prepared (1×10^4 cells/mL) and seeded into low-attachment 6-well plates in serum-free DMEM/F12 (Gibco, Thermo Fisher Scientific, Waltham, MA, USA, Cat. No. 11320033) containing 20 ng/mL EGF (Gibco™, Thermo Fisher Scientific, Waltham, MA, USA, Cat. No. PHG0311), 10 ng/mL bFGF (Thermo Fisher Scientific, Waltham, MA, USA, Cat. No. 13256-029), and B27 (1×) (Thermo Fisher Scientific, Waltham, MA, USA, Cat. No. 17504044). Cells were incubated for 7 days at 37 °C in 5% CO_2, with half of the medium replaced every 3 days. Sphere formation was observed using an inverted microscope (Olympus IX73, Olympus Corporation, Tokyo, Japan). The number of spheres with a diameter >50 µm was recorded, and their diameters were measured. Quantification was conducted using ImageJ. To reduce technical bias, single-cell suspension quality, medium sterility, and consistent microscope settings were maintained during data collection. All sphere formation assays were performed in at least three independent biological replicates, and serum-free medium components were obtained from the same lot to reduce batch-to-batch variation.

Statistical Analysis

Statistical analyses were conducted using GraphPad Prism version 8.0.2. Continuous variables were expressed as mean ± standard deviation (SD). Comparisons between groups were performed using either *t*-tests or one-way ANOVA, as appropriate. Categorical clinicopathologic parameters were analyzed using the Chi-square test, and Fisher's exact test was applied when expected cell counts were below 5. A p-value < 0.05 (two-sided) was considered statistically significant.

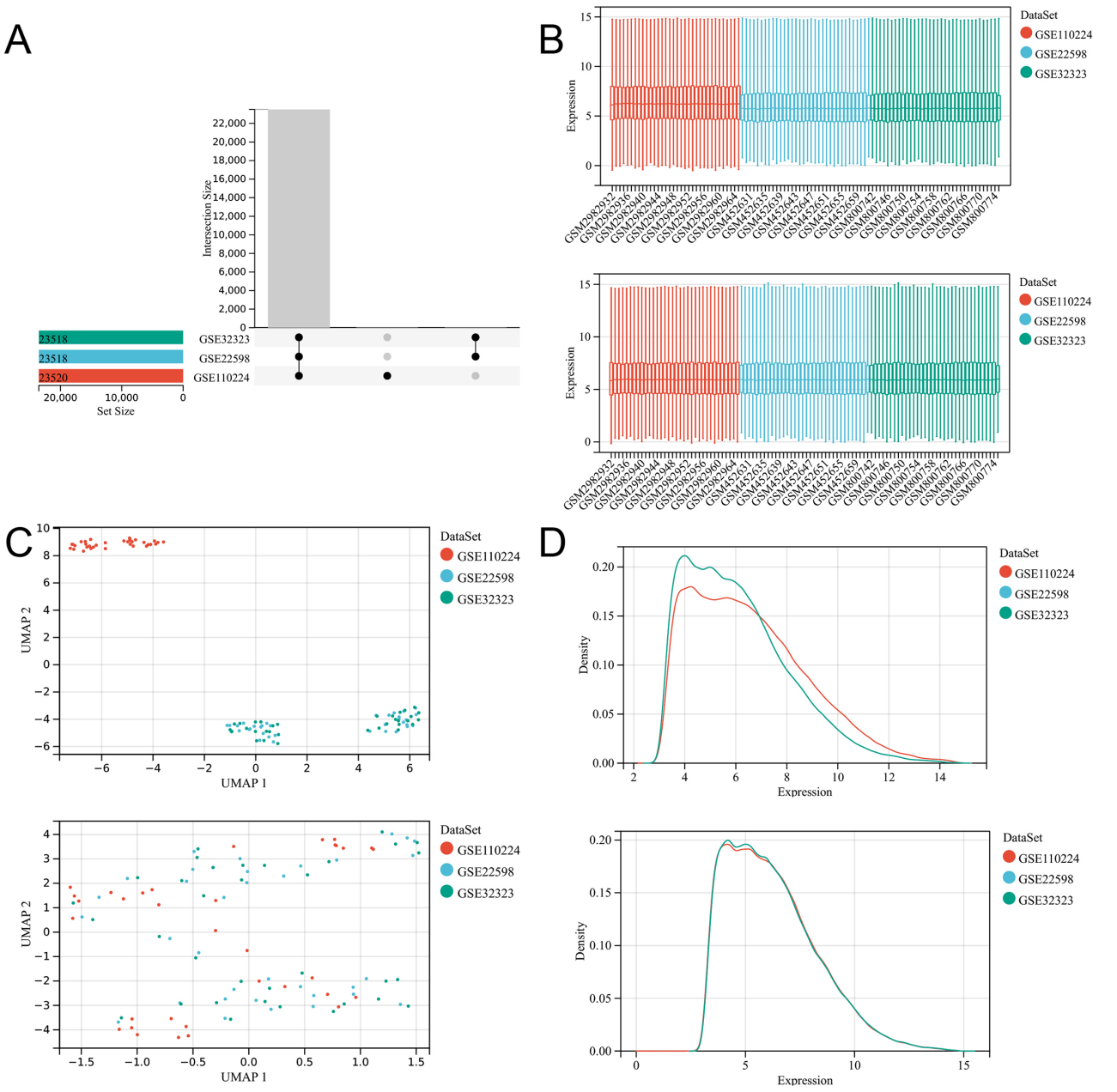

Fig. 1. Integration of multiple CRC datasets from GEO. (A,B) Box plot, (C) UMAP plot, and (D) density plot indicating the patient sample distribution before (upper panel) and after (lower panel) removing the batch effects. CRC, colorectal cancer; UMAP, uniform manifold approximation and projection.

Results

Identification of Differentially Expressed Genes in CRC

Three CRC datasets (GSE110224, GSE22598, and GSE32323) were combined after correcting for batch effects. As shown in Fig. 1A, the intersection among the three datasets was examined, and significant differences among the datasets were observed. Boxplots, UMAP projections, and density plots showed significant between-dataset variation, consistent with batch effects arising from differences in experimental conditions and library preparation methods. These batch effects were effectively reduced using the method reported by Johnson WE *et al.* [22], yielding improved alignment of sample distributions across datasets (Fig. 1B–D).

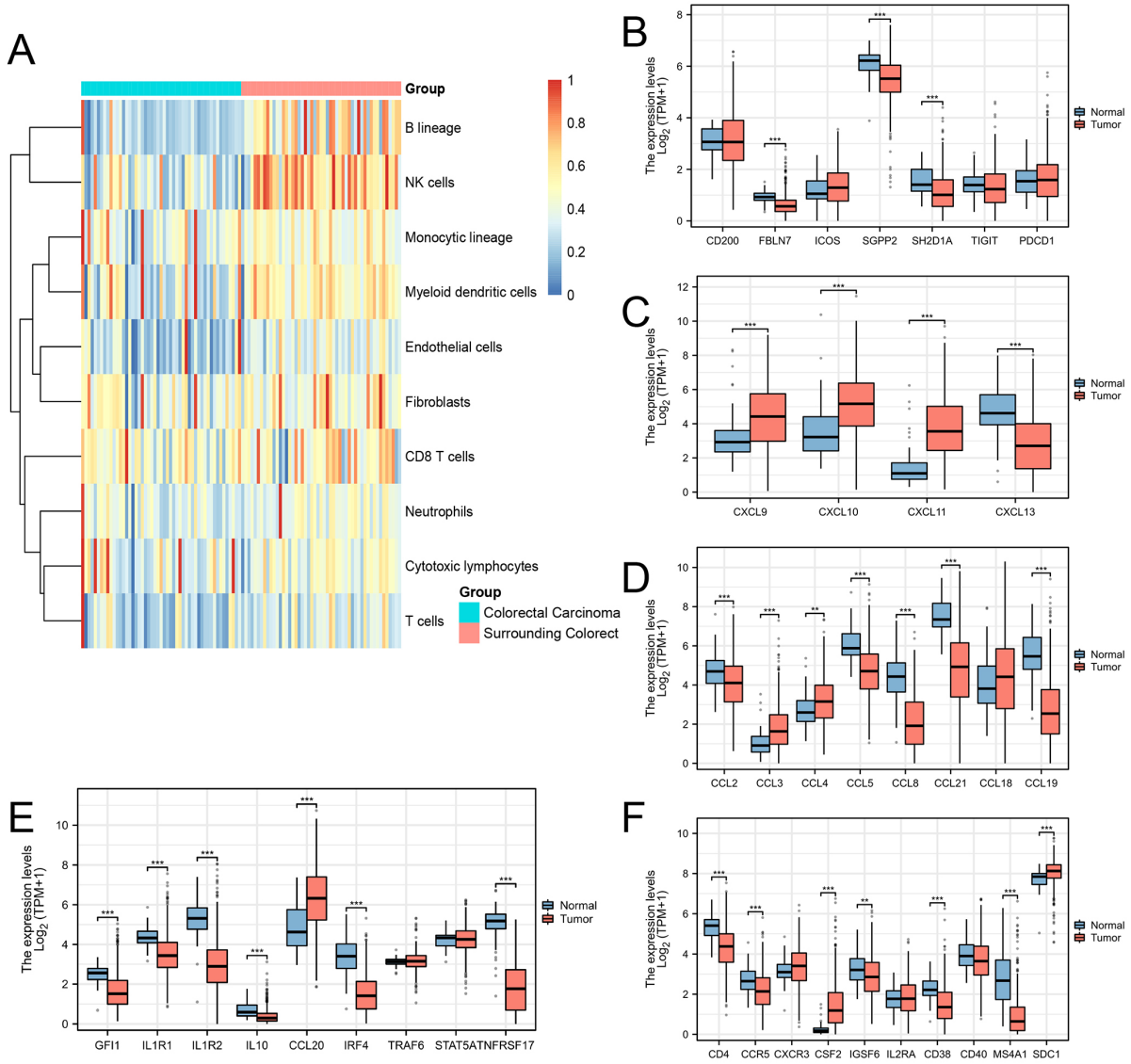

Fig. 2. Immune cell composition and association with TLSs in CRC. (A) The composition of immune cells in the TME of CRC patients. The expression levels of (B) Tfh cell signature genes, (C,D) TLS-related chemokines, and (E,F) TH1/B cell signature genes in CRC and adjacent normal tissues. Asterisks indicate statistical significance (**$p < 0.01$, ***$p < 0.001$). TLSs, tertiary lymphoid structures; TME, tumor microenvironment; Tfh, T follicular helper.

Immune Cell Composition and Association With TLSs in CRC

The tumor microenvironment (TME) plays a crucial role in cancer development and progression, and its cellular composition is associated with immune responses to anti-tumor therapies [25]. We profiled the composition of immune cells in CRC using the merged GEO datasets (Fig. 2A). Overall immune-cell enrichment, especially for B cells, T cells, and neutrophils, was substantially lower in CRC tissues than in adjacent normal samples.

Subsequently, we evaluated the correlation between TLS-associated signature genes and CRC. Several T follicular helper (TFH) signature genes, including FBLN7, SGPP2, and SH2D1A, were downregulated in CRC, whereas *CD200*, *ICOS*, *TIGIT* and *PDCD1* showed no significant differences between CRC and normal adjacent tissues (Fig. 2B). Moreover, analysis of TLS-related chemokines revealed that *CXCL9*, *CXCL10*, *CXCL11*, *CCL3* and *CCL4* were upregulated, while *CXCL13*, *CCL2*, *CCL5*, *CCL8*, *CCL21*, and *CCL19* were downregulated in CRC (Fig. 2C,D). Furthermore, expression analysis of TH1B signature genes indicated that *GFI1*, *IL1R1*, *IL1R2*, *IL10*, *IRF4*, *TNFRSF17*, *CD4*, *CCR5*, *IGSF6*, *CD38*, and *MS4A1* were downregulated, while *CCL20*, *CSF2*, and *SDC1* were upregulated in CRC tissues (Fig. 2E,F).

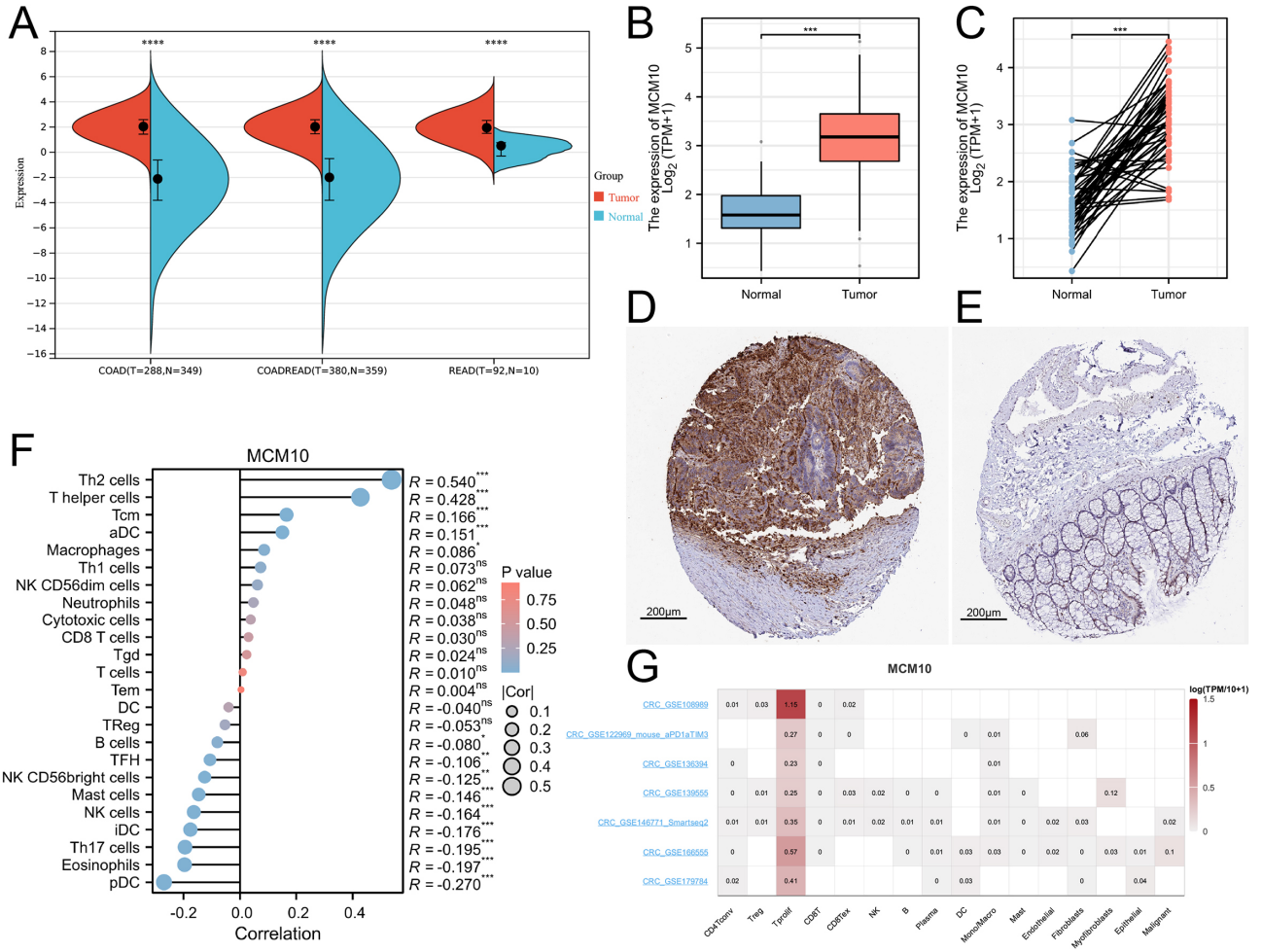

Fig. 3. Expression levels of *MCM10* in CRC at the molecular and tissue levels. (A) MCM10 expression in COAD, COADREAD, and READ samples and normal adjacent tissues in TCGA and GTEx databases. (B) MCM10 expression in unpaired CRC and normal tissues in the TCGA database. (C) MCM10 expression in paired CRC and normal tissues in the TCGA database. Representative immunohistochemical images showing MCM10 protein expression in (D) CRC tissues and (E) normal colorectal tissues were obtained from the Human Protein Atlas (HPA) database. The data are publicly available on the HPA website under the MCM10 gene entry (https://www.proteinatlas.org/ENSG00000065328-MCM10/cancer/colorectal+cancer) (F) The correlation between MCM10 expression and immune cell infiltration in CRC was analyzed using ssGSEA. (G) The correlation between MCM10 expression and immune cell infiltration in different CRC datasets. Asterisks indicate statistical significance (*$p < 0.05$, **$p < 0.01$, ***$p < 0.001$, ****$p < 0.0001$). ns, not statistically significant; HPA, Human Protein Atlas; ssGSEA, single-sample gene set enrichment analysis.

MCM10 is Differentially Expressed in CRC

The expression pattern of *MCM10* in CRC was assessed using RNA-seq data from the TCGA and GTEx databases. *MCM10* was significantly upregulated in COAD+READ, COAD, and READ samples compared with normal tissues from the GTEx database (Fig. 3A). Similarly, analysis of unpaired TCGA-COAD/READ samples indicated higher *MCM10* expression in CRC (Fig. 3B), and paired tumor-normal comparisons in TCGA further validated this increase in CRC (Fig. 3C).

Immunohistochemical staining results from the HPA database also supported these observations, with a significant abundance of MCM10-positive cells in CRC tissue sections (Fig. 3D) than in adjacent normal tissues (Fig. 3E). Furthermore, the association between *MCM10* levels and immune-cell infiltration in CRC was assessed using the ssGSEA. *MCM10* expression exhibited positive correlation with T helper 2 (Th2) cells (R = 0.54), T helper cells (R = 0.428), central memory T cells (Tcm, R = 0.166), activated dendritic cells (aDC, R = 0.151), and macrophages (R = 0.086). However, it was negatively correlated with plasmacytoid dendritic cells (pDC, R = –0.27), eosinophils (R = –0.197), Th17 cells (R = –0.195), iDC (R = –0.176), MK cells (R = –0.164), mast cells (R = –0.146), NK CD56bright cells (R = –0.125), Tfh cells (R = –0.106), and B cells (R = –0.08) (Fig. 3F). A heatmap indicating association across

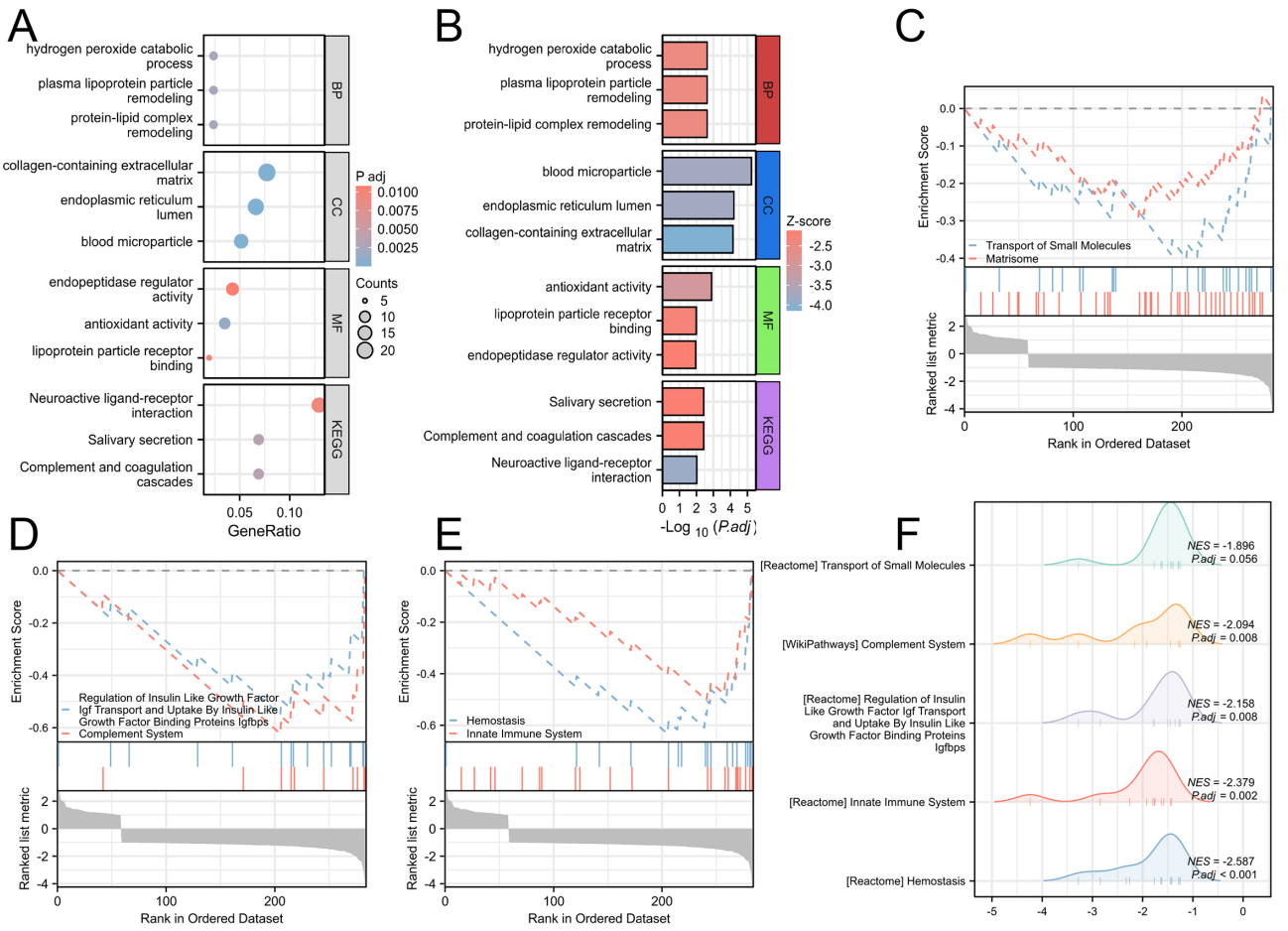

Fig. 4. Enrichment analysis of *MCM10* in CRC. (A,B) GO and KEGG enrichment analysis of DEGs between the low- and high-MCM10 CRC subgroups in TCGA-COAD and TCGA-READ. (C–F) Gene Set Enrichment Analysis (GSEA) of identified DEGs. DEGs, differentially expressed genes.

several CRC datasets further demonstrated that MCM10 expression was consistently positively correlated with T-proliferating cell infiltration (Fig. 3G). Overall, these findings indicate that *MCM10* is upregulated in CRC and is associated with distinct patterns of immune-cell infiltration.

Enrichment Analysis of MCM10 in CRC

DEGs between the high or low-*MCM10* CRC groups were identified using TCGA-COAD and TCGA-READ. Then, GSEA was performed to decipher *MCM10*-related CRC hallmarks, and functional enrichment analyses were conducted for the identified DEGs.

GO analysis revealed that *MCM10* expression was significantly associated with biological processes, including hydrogen peroxide catabolism, plasma lipoprotein particle remodeling, and protein-lipid complex remodeling. Enriched cellular components included the collagen-containing ECM, endoplasmic reticulum lumen, and blood microparticle. Enriched molecular functions involved endopeptidase regulator activity, antioxidant activity, and lipoprotein particle receptor binding. Furthermore, KEGG enrichment analyses suggested links between *MCM10* and signaling pathways related to neuroactive ligand-receptor interaction, salivary secretion, and complement and coagulation cascades (Fig. 4A,B). Consistent with these findings, GSEA revealed significant enrichment of gene sets correlated with the complement system, endocrine system, immune system, and hemostasis (Fig. 4C–F).

Association of MCM10 With Clinical Features of CRC Patients

The pan-cancer expression profile of *MCM10* was evaluated using TCGA dataset. *MCM10* was found to be upregulated across several types of cancer, including bladder cancer, breast cancer, colorectal cancer, among others (Fig. 5A). Moreover, we found that the expression pattern showed significant difference in different clinical phenotypes. As illustrated in Fig. 5B, *MCM10* expression level was lower in patients with a history of colon polyps, those with lymphatic invasion, and those with a BMI >25.

Furthermore, *MCM10* levels were significantly correlated with pathologic N stage ($p = 0.037$), overall pathologic stage (I–IV) ($p = 0.037$), and a history of colon polyps ($p < 0.001$, Table 1). ROC curve analysis yielded an AUC of

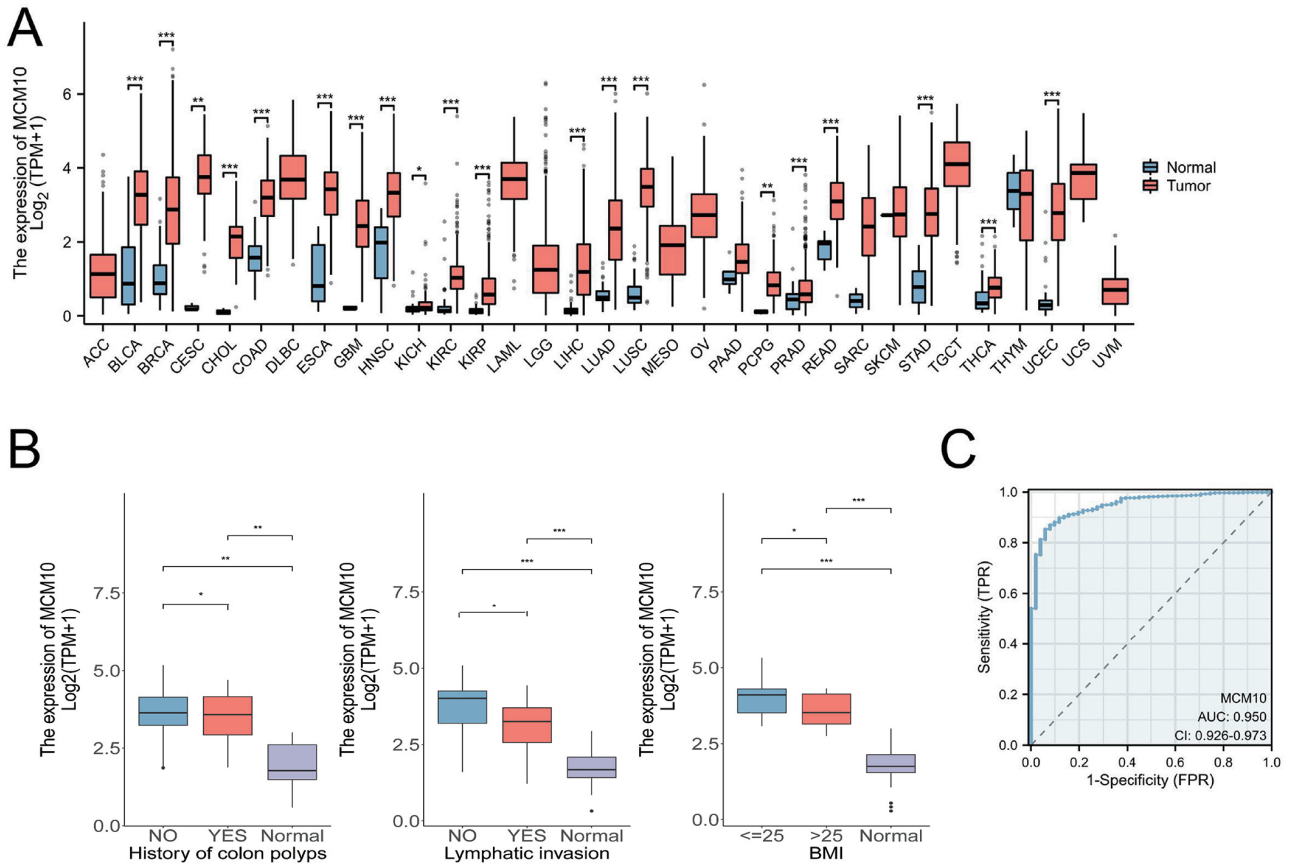

Fig. 5. Pan-cancer *MCM10* expression and correlation with clinical features of CRC patients. (A) Pan-cancer expression pattern of MCM10 in the TCGA database. (B) The MCM10 expression in CRC patients with different clinical phenotypes. (C) ROC curve analysis was used to evaluate the diagnostic performance of MCM10 in CRC. Asterisks indicate statistical significance (*$p < 0.05$, **$p < 0.01$, ***$p < 0.001$).

0.950 (95% CI: 0.926–0.973), suggesting strong diagnostic performance of *MCM10* for differentiating CRC from normal tissues (Fig. 5C).

Identification of Molecular Subtypes and Correlation With Gene Mutation

Given the altered expression of TLS signature genes in the CRC tumor microenvironment, we further investigated TLS-related molecular subtypes. Differential expression of TLS-related genes between CRC and normal tissues was visualized by heatmap (Fig. 6A). Based on consensus clustering of TLS signature genes, patients were stratified into two subgroups: C1 (TLS-positive) and C2 (TLS-negative) (Fig. 6B). TLS signature genes were significantly upregulated in the C1 subgroup (Fig. 6C). Mutation analysis revealed no significant differences in the frequencies of driver gene mutations between the two subgroups (Fig. 6D).

We identified 424 upregulated and 11 downregulated DEGs between C1 and C2 (Fig. 6E). GO enrichment analysis of the upregulated genes indicated their roles in cell activation, immunoglobulin-mediated responses, and leukocyte-mediated immunity, whereas KEGG analysis revealed significant enrichment in pathways associated with bacterial infection and immune-related diseases (Fig. 6F). In contrast, the downregulated genes were primarily associated with immune-cell migration and chemokine activity, and KEGG analysis indicated enrichment in the IL-17 signaling pathway and sulfur metabolism (Fig. 6G).

MCM10 Expression in CRC and Its Impact on Cell Viability, Invasion, and Migration

The role of MCM10 in CRC was further validated through multiple experiments. qRT-PCR and Western blot analyses revealed that *MCM10* mRNA and protein levels were significantly upregulated in HCT116 and SW480 compared to FHC, with the higher expression observed in the HCT116 group (Fig. 7A,B). In HCT116 cells, its expression was significantly reduced in the sh-MCM10 group and substantially elevated in the oe-MCM10 group at both mRNA and protein levels. However, no significant differences were observed between the sh-NC and oe-NC groups (Fig. 7C,D).

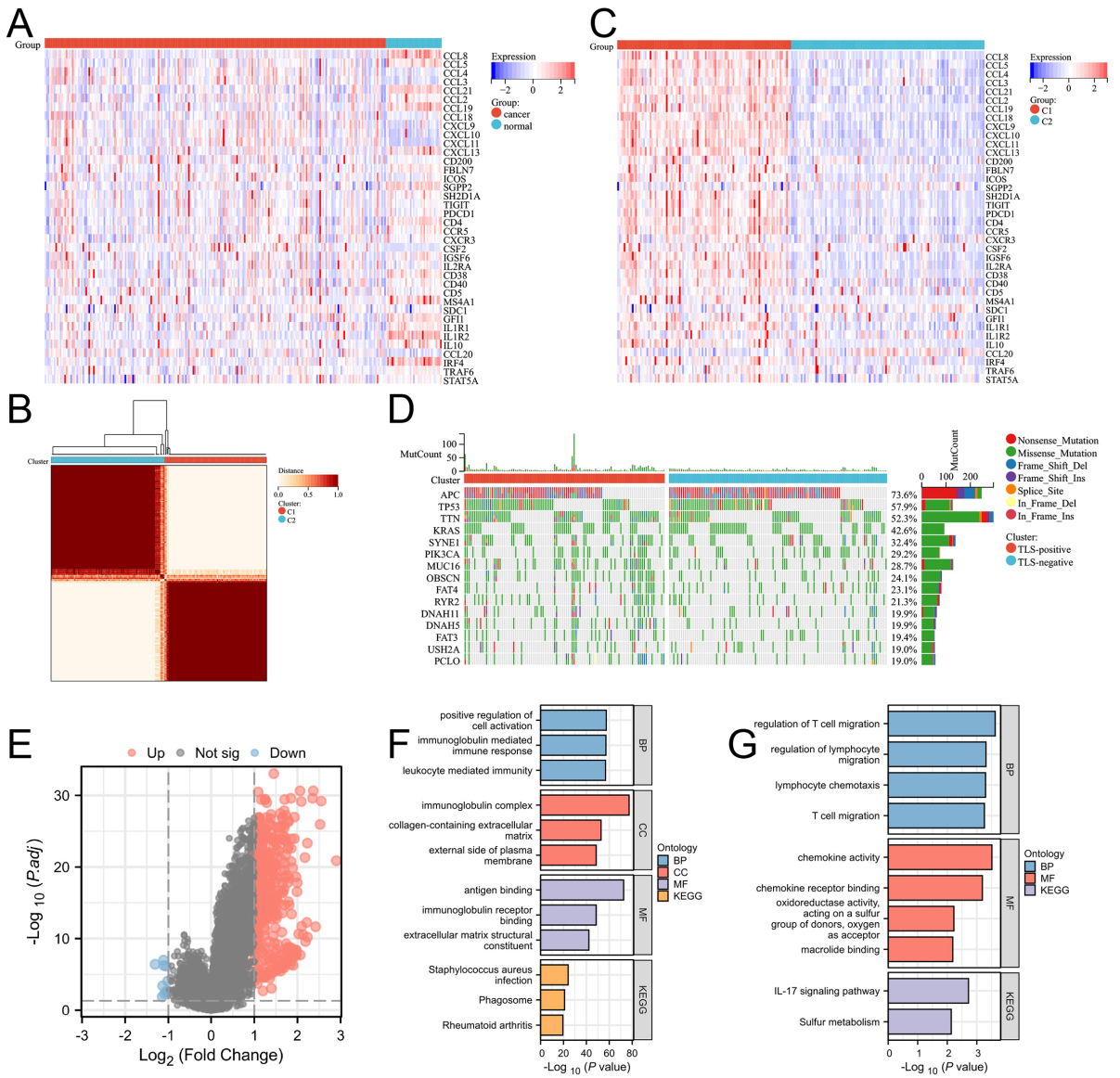

Fig. 6. TLS-related molecular subtypes in CRC. (A) Differential expression levels of TLS-related genes in the CRC and normal adjacent tissues are displayed as a heatmap. (B) Consensus clustering was performed to divide the CRC patients into the C1 and C2 clusters. (C) The expression levels of TLS-related genes in the C1 and C2 clusters was shown in a heatmap. (D) The landscape of gene mutation status in C1 and C2 clusters. (E) Volcano plot of the DEGs between the C1 and C2 clusters. GO and KEGG analyses of (F) upregulated genes and (G) downregulated genes between the C1 and C2 clusters. GO, gene ontology.

MTT assay results showed that the viability of sh-MCM10 cells was significantly reduced compared to the sh-NC group, whereas the viability of oe-MCM10 cells was significantly increased compared with the oe-NC group. Moreover, cellular viability increased over time in all groups (Fig. 7E). Transwell assays further demonstrated that the invasion and migration capabilities were significantly reduced in sh-MCM10 cells compared with the sh-NC group; in contrast, cellular migration and invasion were significantly increased in oe-MCM10 cells compared to the oe-NC group (Fig. 7F,G).

MCM10 Regulated the Sphere-Forming Capacity and Expression of Key Proteins

The results demonstrated that *MCM10* expression significantly affected stemness-related properties in HCT116 cells. In the sphere formation assay, *MCM10* knockdown (sh-MCM10) significantly reduced sphere formation, whereas *MCM10* overexpression (oe-MCM10) markedly enhanced sphere-forming capacity compared with their respective control groups. Quantitative analysis confirmed a significant decrease in the number of tumor spheres in the sh-MCM10 group and a significant increase in the oe-MCM10 group (Fig. 8A).

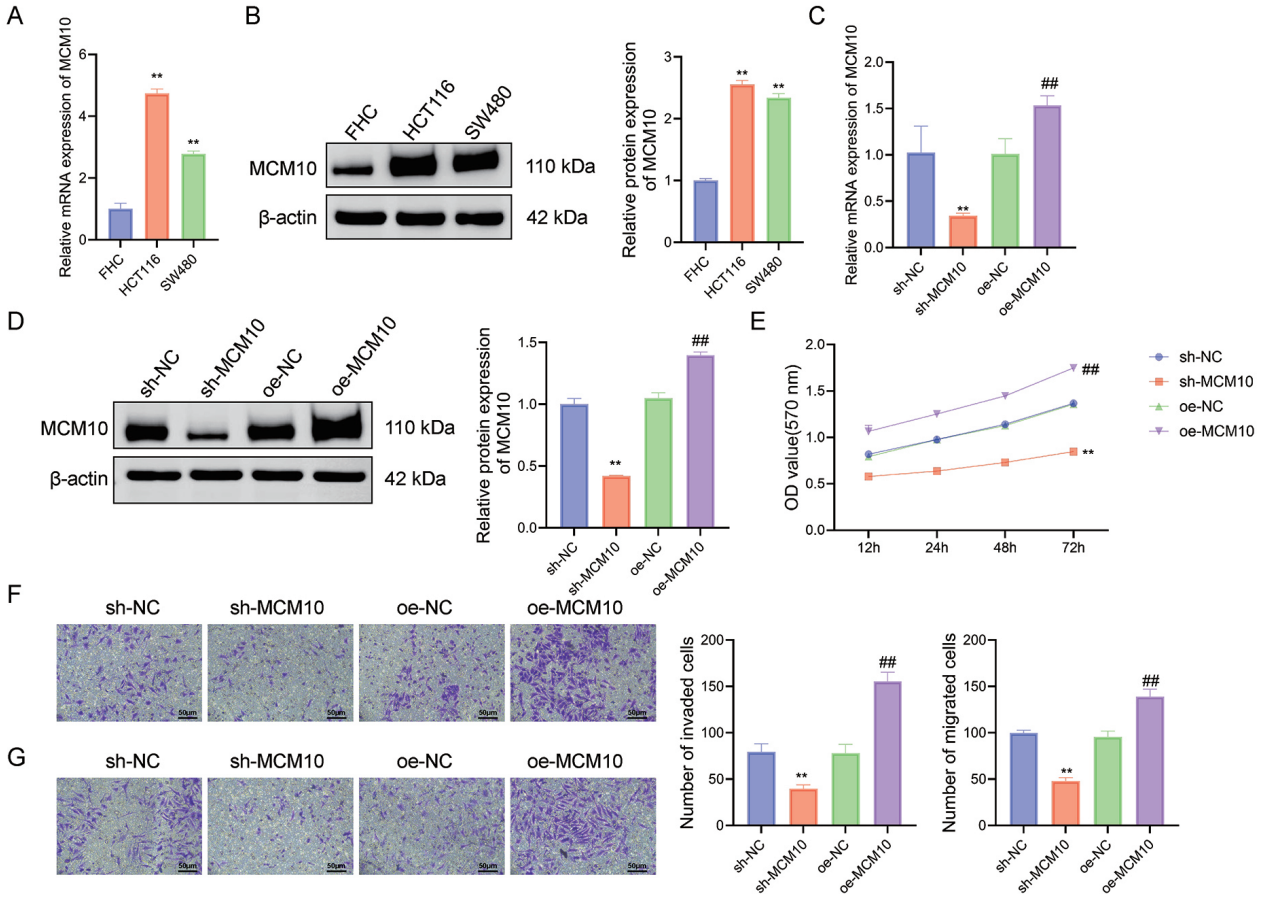

Fig. 7. MCM10 expression in colorectal cancer and its impact on cell viability, invasion, and migration. (A) Detection of MCM10 expression levels in FHC, HCT116, and SW480 cells. (B) MCM10 protein expression levels in FHC, HCT116, and SW480 cells. (C) *MCM10* expression levels in sh-NC, sh-MCM10, oe-NC, and oe-MCM10 groups. (D) MCM10 protein expression levels in sh-NC, sh-MCM10, oe-NC, and oe-MCM10 groups. (E) Cell viability changes in sh-NC, sh-MCM10, oe-NC, and oe-MCM10 groups. (F) Cell invasion capability in sh-NC, sh-MCM10, oe-NC, and oe-MCM10 groups. (G) Cell migration capability in sh-NC, sh-MCM10, oe-NC, and oe-MCM10 groups. Data are presented as mean ± SD from three independent biological experiments (n = 3). ** indicated $p < 0.01$ compared with sh-NC; ## indicated $p < 0.01$ compared with oe-NC. FHC, fetal human colonic epithelial cells; oe-NC, overexpression negative control.

Western blot analysis revealed that the expression levels of stemness-related proteins, including SOX2, Oct4, NANOG, and KLF4, were significantly downregulated in the sh-MCM10 group compared with the sh-NC group, whereas their expression levels were upregulated in the oe-MCM10 group compared with the oe-NC group (Fig. 8B). Quantitative analysis showed that the expression levels of SOX2, Oct4, NANOG, and KLF4 were markedly reduced in the sh-MCM10 group, whereas they were substantially increased in the oe-MCM10 group. No significant differences were observed between the sh-NC and oe-NC groups (Fig. 8C). These findings suggest that *MCM10* regulates the expression levels of stemness-related proteins and significantly modulates the sphere-forming capacity of colorectal cancer cells, providing critical evidence for further investigation of *MCM10* in cancer stem cells.

Discussion

Colorectal cancer is the third leading cause of cancer-related death worldwide. Genetic alterations play a vital role in CRC pathogenesis, and accumulated DNA mutations can drive the progression of both sporadic and hereditary forms of the disease [26]. *MCM10* is a key factor required for DNA replication in eukaryotes, and its dysregulation can contribute to carcinogenesis [27]. In this study, we found differential expression of TLS-related signature genes in CRC and, through transcriptomic analyses of public databases, observed that MCM10 is upregulated in CRC tissues. Furthermore, we identified correlations between MCM10 levels and patterns of immune-cell infiltration, indicating that MCM10 might be a novel prognostic and therapeutic biomarker in CRC [28]. However, since TCGA and GTEx samples differ in demographic character-

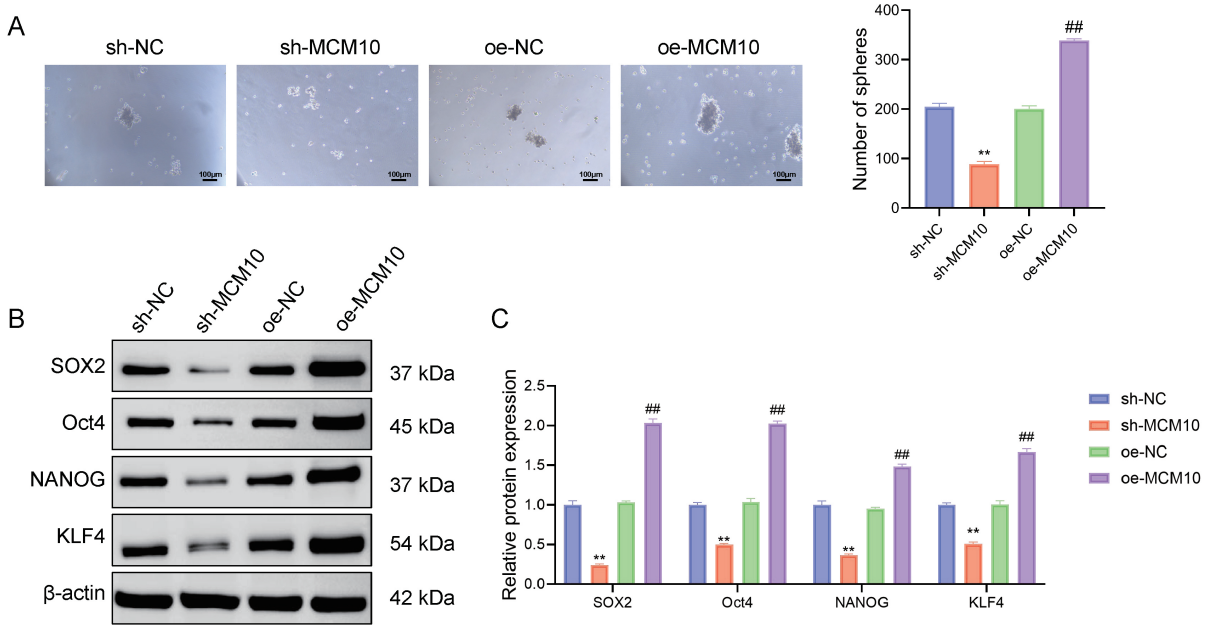

Fig. 8. Detection of sphere-forming capacity and expression of key proteins. (A) Representative images and quantitative analysis of sphere formation in different groups. (B) Detection of proteins (SOX2, Oct4, NANOG, KLF4) in different groups. (C) Relative expression analysis of proteins in different groups. Data are presented as mean ± SD from three independent biological experiments (n = 3). ** indicated $p < 0.01$ compared with sh-NC; ## indicated $p < 0.01$ compared with oe-NC. SOX2, SRY-box transcription factor 2; Oct4, octamer-binding transcription factor 4; NANOG, NANOG homeobox; KLF4, Kruppel-like factor 4.

istics and tissue collection protocols, residual confounding cannot be fully excluded when comparing tumor and normal tissues.

Cancer-related immunity affects tumor development and progression, response to therapy, and overall clinical outcome [29]. Although lymph nodes are well recognized as the primary site of anti-tumor immunity, increasing evidence revealed that TLSs can contribute to the induction or reactivation of anti-cancer immunity [30], and serve as a positive prognostic marker in various malignancies [28,31]. TLSs resemble lymph nodes in both structure and developmental processes and contain diverse immune-cell subsets [30]. Therefore, transcriptomic signatures have been proposed to detect TLS presence and maturity.

Several chemokines and immune signatures are closely associated with TLS biology. For example, *CXCL13*, a key B-cell-attracting chemokine, is strongly associated with TLS formation. CXCL13-producing Thf cells are enriched within TLSs and promote the activation and organization of local T-cell-mediated immunity. Other chemokines, including *CCL2*, *CCL3*, *CCL4*, and *CCL8*, are related to B and T-cell chemotaxis and have been reported across various TLS maturation stages [32]. Moreover, the Th1/B cell-associated signature genes such as *CCR5*, *CXCR3*, *IL1R1*, *IL1R2*, and *IL10* are implicated in the proliferation of B cells or T cells, and are associated with T-cell activation and Th cell differentiation [33].

In this study, we evaluated immune-cell composition in the TME of CRC. Infiltration of key immune cells, particularly T cells and B cells, was decreased in tumor tissues relative to the surrounding normal tissues, consistent with an immunosuppressive microenvironment. The expression of many signature genes associated with Thf cells, Th1/B cells, and chemokines was significantly downregulated in CRC. Notably, some signature genes, such as *CCL3*, *CCL4*, and *CCL20*, showed upregulation in CRC, and were in line with the previous research [34]. Furthermore, consensus clustering was performed using TLS signature genes, and CRC patients were divided into the TLS-positive and TLS-negative clusters. Differential expression analysis between these clusters revealed genes enriched for pathways associated with lymphocyte activation and migration. These findings should be interpreted cautiously, as MCPcounter provides only signature-based estimates with limited resolution for specific immune-cell subtypes and does not fully reflect cellular heterogeneity within the TME.

Our study demonstrated that MCM10 expression levels were positively correlated with Th2 cells (R = 0.540), overall Th cells, central memory cells (Tcm), and aDCs, while showing negative associations with pDCs, Th17 cells, and NK cells. These findings suggest that MCM10 may play an immunomodulatory role within the tumor immune microenvironment. Previous studies have shown that upregulation of Th2 cells is often associated with an im-

munosuppressive tumor state, promoting immune evasion by inhibiting Th1-type cytotoxic responses [35,36]. Additionally, the positive association between MCM10 and Tcm cells may help maintain the weakly immunogenic "cold tumor" phenotype. In contrast, the negative correlations with NK cells and Th17 cells, both of which can contribute to antitumor properties, further support the hypothesis that increased MCM10 is associated with immune suppression. Collectively, these findings suggest that high *MCM10* expression may not only enhance aggressive tumor behavior but also facilitate CRC progression by remodeling the immune microenvironment in ways that favor immune evasion.

MCM10 serves as a firing (activating) factor of the DNA replication origin and has been linked to replication catastrophe, which can result in genomic instability and ultimately carcinogenesis [37,38]. Substantial evidence indicated that MCM10 is overexpressed in multiple cancer types and demonstrates oncogenic activity that supports cancer progression. For example, MCM10 is highly expressed in breast cancer and facilitates cellular proliferation, migration, and invasion through activation of the Wnt/β-catenin pathway [39]. Similarly, increased MCM10 expression in prostate cancer has been associated with enhanced proliferation and reduced apoptosis [40]. Additionally, pan-cancer analysis revealed that MCM10 is a reliable biomarker with diagnostic and prognostic values in the pan-cancer analysis [41,42].

Consistent with these reports, our study identified that MCM10 is substantially upregulated in CRC tissues relative to the adjacent normal tissues. Notably, recent CRC-specific studies also support the biological relevance of MCM10 in colorectal tumorigenesis. Lu *et al.* [21] reported that MCM10 is strongly associated with chromosomal instability and stemness-related transcriptional programs in CRC. Moreover, MCM10 has been implicated in sustaining Myc-driven replication stress [38], a pathway closely linked to Wnt/β-catenin signaling, suggesting that aberrant MCM10 expression may cooperate with canonical oncogenic pathways in CRC. Consistent with this pattern, our co-expression and enrichment analyses further indicated that MCM10-related genes were predominantly enriched in pathways associated with molecular transport and immune regulation. Furthermore, ROC analysis supported the diagnostic potential of MCM10 in CRC, yielding an AUC of 0.95. The variation in the 95% CI likely reflects cross-platform differences between TCGA tumor samples and GTEx normal tissues, which can affect the stability of ROC estimation, rather than indicating overfitting.

Our *in vitro* experimental results further confirmed the critical role of MCM10 in CRC, particularly in promoting tumor progression and sustaining stemness-related phenotypes. qRT-PCR and Western blot analyses revealed that *MCM10* mRNA and protein levels were significantly higher in HCT116 and SW480 compared to FHC. Additionally, functional experiments further clarified its specific oncogenic effects: MCM10 knockdown (sh-MCM10) significantly decreased cell viability, invasion, and migration, whereas MCM10 overexpression (oe-MCM10) improved these behaviors. These results were consistent with previous studies, including findings in gastric cancer [43], where high MCM10 expression has been shown to enhance the migratory and invasive capabilities of cancer cells and promote resistance to apoptosis.

To further investigate the impact of MCM10 on CRC stemness, we conducted sphere formation assays and analyzed the expression of stemness-related proteins. The results indicated that MCM10 might enhance the stemness of CRC cells by regulating the expression of stemness-associated proteins, thereby supporting tumor maintenance and progression. Nevertheless, our experimental workflow was limited to HCT116 and SW480 cell lines, which cannot fully represent major CRC molecular subtypes, such as MSI or CMS. Future studies should incorporate additional subtype-representative cell lines and patient-derived CRC models to improve generalizability. Overall, by integrating bioinformatics/transcriptomic analyses with experimental validation, this study highlights the critical role of MCM10 in CRC and supports its potential as a reliable diagnostic, immunological, and prognostic biomarker, as well as a candidate therapeutic target.

Although this study underscores the significance of MCM10 in CRC through integrated bioinformatic analyses and experimental validation, several limitations remain to be addressed. First, the study primarily relies on *in vitro* experiments and bioinformatic analyses of publicly available databases, with limited validation in *in vivo* models, which may limit the applicability of the findings. Second, while the study identified a strong correlation between MCM10 and immune-cell infiltration as well as stemness-associated protein expression, the precise regulatory mechanisms remain unclear, particularly whether MCM10 exerts its effects through specific signaling pathways.

Future studies should therefore: (i) validate the role of MCM10 in tumorigenesis and immune regulation using appropriate animal models; (ii) elucidate the interaction of MCM10 with key signaling pathways and its molecular mechanisms in tumor resistance and recurrence; (iii) conduct multicenter studies to determine the diagnostic and prognostic utility of MCM10 in CRC; and (iv) develop and assess MCM10-targeted interventions, such as small-molecule inhibitors or RNA-based techniques, both as monotherapies or in combination regimens.

Conclusion

In summary, our findings demonstrate that *MCM10* is significantly overexpressed in colorectal cancer and is strongly associated with immune-cell infiltration, enhanced tumor cell proliferation, migration, invasion, and stemness.

Functional enrichment analyses further linked *MCM10* to key cancer-related signaling and immune regulatory pathways. These results underscore the potential of *MCM10* as a promising diagnostic and prognostic biomarker and provide a rationale for future studies investigating it as a therapeutic target in colorectal cancer.

Abbreviations

CRC, colorectal cancer; TLSs, Tertiary lymphoid structures; MCMs, Minichromosome maintenance proteins; MCPcounter, Microenvironment Cell Populations-counter; HPA, Human Protein Atlas; ssGSEA, single-sample GSEA; BCA, bicinchoninic acid.

Availability of Data and Materials

The datasets used and/or analyzed during the current study are available from the corresponding author on reasonable request.

Author Contributions

All authors contributed to the study conception and design. Material preparation, data collection and analysis were performed by SKW and CFY. The first draft of this manuscript was written by CZ, YLL and BBC. All authors commented on and critically revised previous versions of the manuscript. All authors read and approved the final manuscript. All authors agreed to be accountable for all aspects of the work in ensuring that questions related to the accuracy or integrity of any part of the work are appropriately investigated and resolved.

Ethics Approval and Consent to Participate

Not applicable.

Acknowledgment

Not applicable.

Funding

This study was supported by Nn10 Program of Harbin Medical University Cancer Hospital (No. Nn102017-02).

Conflict of Interest

The authors declare no conflict of interest.

References

[1] Sung H, Ferlay J, Siegel RL, Laversanne M, Soerjomataram I, Jemal A, *et al*. Global Cancer Statistics 2020: GLOBOCAN Estimates of Incidence and Mortality Worldwide for 36 Cancers in 185 Countries. CA: A Cancer Journal for Clinicians. 2021; 71: 209–249. https://doi.org/10.3322/caac.21660.

[2] Dekker E, Tanis PJ, Vleugels JLA, Kasi PM, Wallace MB. Colorectal cancer. Lancet (London, England). 2019; 394: 1467–1480. https://doi.org/10.1016/S0140-6736(19)32319-0.

[3] Weng J, Li S, Zhu Z, Liu Q, Zhang R, Yang Y, *et al*. Exploring immunotherapy in colorectal cancer. Journal of Hematology & Oncology. 2022; 15: 95. https://doi.org/10.1186/s13045-022-01294-4.

[4] Biller LH, Schrag D. Diagnosis and Treatment of Metastatic Colorectal Cancer: A Review. JAMA. 2021; 325: 669–685. https://doi.org/10.1001/jama.2021.0106.

[5] Chibaudel B, Tournigand C, Bonnetain F, Richa H, Benetkiewicz M, André T, *et al*. Therapeutic strategy in unresectable metastatic colorectal cancer: an updated review. Therapeutic Advances in Medical Oncology. 2015; 7: 153–169. https://doi.org/10.1177/1758834015572343.

[6] Galon J, Costes A, Sanchez-Cabo F, Kirilovsky A, Mlecnik B, Lagorce-Pagès C, *et al*. Type, density, and location of immune cells within human colorectal tumors predict clinical outcome. Science (New York, N.Y.). 2006; 313: 1960–1964. https://doi.org/10.1126/science.1129139.

[7] Bindea G, Mlecnik B, Tosolini M, Kirilovsky A, Waldner M, Obenauf AC, *et al*. Spatiotemporal dynamics of intratumoral immune cells reveal the immune landscape in human cancer. Immunity. 2013; 39: 782–795. https://doi.org/10.1016/j.immuni.2013.10.003.

[8] Berntsson J, Nodin B, Eberhard J, Micke P, Jirström K. Prognostic impact of tumour-infiltrating B cells and plasma cells in colorectal cancer. International Journal of Cancer. 2016; 139: 1129–1139. https://doi.org/10.1002/ijc.30138.

[9] Sautès-Fridman C, Petitprez F, Calderaro J, Fridman WH. Tertiary lymphoid structures in the era of cancer immunotherapy. Nature Reviews. Cancer. 2019; 19: 307–325. https://doi.org/10.1038/s41568-019-0144-6.

[10] Lauss M, Donia M, Svane IM, Jönsson G. B Cells and Tertiary Lymphoid Structures: Friends or Foes in Cancer Immunotherapy? Clinical Cancer Research: an Official Journal of the American Association for Cancer Research. 2022; 28: 1751–1758. https://doi.org/10.1158/1078-0432.CCR-21-1130.

[11] Zhang Q, Wu S. Tertiary lymphoid structures are critical for cancer prognosis and therapeutic response. Frontiers in Immunology. 2023; 13: 1063711. https://doi.org/10.3389/fimmu.2022.1063711.

[12] Zhang C, Wang XY, Zuo JL, Wang XF, Feng XW, Zhang B, *et al*. Localization and density of tertiary lymphoid structures associate with molecular subtype and clinical outcome in colorectal cancer liver metastases. Journal for Immunotherapy of Cancer. 2023; 11: e006425. https://doi.org/10.1136/jitc-2022-006425.

[13] Overacre-Delgoffe AE, Bumgarner HJ, Cillo AR, Burr AHP, Tometich JT, Bhattacharjee A, *et al*. Microbiota-specific T follicular helper cells drive tertiary lymphoid structures and anti-tumor immunity against colorectal cancer. Immunity. 2021; 54: 2812–2824.e4. https://doi.org/10.1016/j.immuni.2021.11.003.

[14] Feng H, Yang F, Qiao L, Zhou K, Wang J, Zhang J, *et al*. Prognostic Significance of Gene Signature of Tertiary Lymphoid Structures in Patients With Lung Adenocarcinoma. Frontiers in Oncology. 2021; 11: 693234. https://doi.org/10.3389/fonc.2021.693234.

[15] Wohlschlegel JA, Dhar SK, Prokhorova TA, Dutta A, Walter JC. Xenopus Mcm10 binds to origins of DNA replication after Mcm2-7 and stimulates origin binding of Cdc45. Molecular Cell. 2002; 9: 233–240. https://doi.org/10.1016/s1097-2765(02)00456-2.

[16] Baxley RM, Bielinsky AK. Mcm10: A Dynamic Scaffold at Eukaryotic Replication Forks. Genes. 2017; 8: 73. https://doi.org/10.3390/genes8020073.

[17] Gou K, Liu J, Feng X, Li H, Yuan Y, Xing C. Expression of Minichromosome Maintenance Proteins (MCM) and Cancer Prognosis: A meta-analysis. Journal of Cancer. 2018; 9: 1518–1526. https://doi.org/10.7150/jca.22691.

[18] Han W, Wu YZ, Zhao XY, Gong ZH, Shen GL. Integrative Analysis of Minichromosome Maintenance Proteins and Their Prognostic Significance in Melanoma. Frontiers in Oncology. 2021; 11: 715173. https://doi.org/10.3389/fonc.2021.715173.

[19] Panakkal N, Lekshmi A, Krishna KMJ, Saraswathy VV, Sujathan K. Expression of minichromosome maintenance proteins in the exfoliated cells supplement sputum cytology in the diagnosis of lung cancer. CytoJournal. 2024; 21: 81. https://doi.org/10.25259/Cytojournal_115_2024.

[20] Tian J, Lu Z, Niu S, Zhang S, Ying P, Wang L, *et al*. Aberrant MCM10 SUMOylation induces genomic instability mediated by a genetic variant associated with survival of esophageal squamous cell carcinoma. Clinical and Translational Medicine. 2021; 11: e485. https://doi.org/10.1002/ctm2.485.

[21] Lu Y, Zhou X, Liu Z, Wang W, Li F, Fu W. Characteristic Analysis of Featured Genes Associated With Stemness Indices in Colorectal Cancer. Frontiers in Molecular Biosciences. 2020; 7: 563922. https://doi.org/10.3389/fmolb.2020.563922.

[22] Johnson WE, Li C, Rabinovic A. Adjusting batch effects in microarray expression data using empirical Bayes methods. Biostatistics (Oxford, England). 2007; 8: 118–127. https://doi.org/10.1093/biostatistics/kxj037.

[23] Becht E, Giraldo NA, Lacroix L, Buttard B, Elarouci N, Petitprez F, *et al*. Estimating the population abundance of tissue-infiltrating immune and stromal cell populations using gene expression. Genome Biology. 2016; 17: 218. https://doi.org/10.1186/s13059-016-1070-5.

[24] Wilkerson MD, Hayes DN. ConsensusClusterPlus: a class discovery tool with confidence assessments and item tracking. Bioinformatics (Oxford, England). 2010; 26: 1572–1573. https://doi.org/10.1093/bioinformatics/btq170.

[25] Pitt JM, Marabelle A, Eggermont A, Soria JC, Kroemer G, Zitvogel L. Targeting the tumor microenvironment: removing obstruction to anticancer immune responses and immunotherapy. Annals of Oncology: Official Journal of the European Society for Medical Oncology. 2016; 27: 1482–1492. https://doi.org/10.1093/annonc/mdw168.

[26] Jin K, Ren C, Liu Y, Lan H, Wang Z. An update on colorectal cancer microenvironment, epigenetic and immunotherapy. International Immunopharmacology. 2020; 89: 107041. https://doi.org/10.1016/j.intimp.2020.107041.

[27] Thu YM, Bielinsky AK. Enigmatic roles of Mcm10 in DNA replication. Trends in Biochemical Sciences. 2013; 38: 184–194. https://doi.org/10.1016/j.tibs.2012.12.003.

[28] Goc J, Germain C, Vo-Bourgais TKD, Lupo A, Klein C, Knockaert S, *et al*. Dendritic cells in tumor-associated tertiary lymphoid structures signal a Th1 cytotoxic immune contexture and license the positive prognostic value of infiltrating CD8+ T cells. Cancer Research. 2014; 74: 705–715. https://doi.org/10.1158/0008-5472.CAN-13-1342.

[29] Yoon PS, Del Piccolo N, Shirure VS, Peng Y, Kirane A, Canter RJ, *et al*. Advances in Modeling the Immune Microenvironment of Colorectal Cancer. Frontiers in Immunology. 2021; 11: 614300. https://doi.org/10.3389/fimmu.2020.614300.

[30] Fridman WH, Meylan M, Pupier G, Calvez A, Hernandez I, Sautès-Fridman C. Tertiary lymphoid structures and B cells: An intratumoral immunity cycle. Immunity. 2023; 56: 2254–2269. https://doi.org/10.1016/j.immuni.2023.08.009.

[31] Horeweg N, Workel HH, Loiero D, Church DN, Vermij L, Léon-Castillo A, *et al*. Tertiary lymphoid structures critical for prognosis in endometrial cancer patients. Nature Communications. 2022; 13: 1373. https://doi.org/10.1038/s41467-022-29040-x.

[32] Gu-Trantien C, Loi S, Garaud S, Equeter C, Libin M, de Wind A, *et al*. CD4$^+$ follicular helper T cell infiltration predicts breast cancer survival. The Journal of Clinical Investigation. 2013; 123: 2873–2892. https://doi.org/10.1172/JCI67428.

[33] Hennequin A, Derangère V, Boidot R, Apetoh L, Vincent J, Orry D, *et al*. Tumor infiltration by Tbet+ effector T cells and CD20+ B cells is associated with survival in gastric cancer patients. Oncoimmunology. 2015; 5: e1054598. https://doi.org/10.1080/2162402X.2015.1054598.

[34] Jia SN, Han YB, Yang R, Yang ZC. Chemokines in colon cancer progression. Seminars in Cancer Biology. 2022; 86: 400–407. https://doi.org/10.1016/j.semcancer.2022.02.007.

[35] Li J, Zeng Z, Wu Q, Chen J, Liu X, Zhang J, *et al*. Immunological modulation of the Th1/Th2 shift by ionizing radiation in tumors (Review). International Journal of Oncology. 2021; 59: 50. https://doi.org/10.3892/ijo.2021.5230.

[36] Ryba-Stanisławowska M. Unraveling Th subsets: insights into their role in immune checkpoint inhibitor therapy. Cellular Oncology (Dordrecht, Netherlands). 2025; 48: 295–312. https://doi.org/10.1007/s13402-024-00992-0.

[37] Yeeles JTP, Deegan TD, Janska A, Early A, Diffley JFX. Regulated eukaryotic DNA replication origin firing with purified proteins. Nature. 2015; 519: 431–435. https://doi.org/10.1038/nature14285.

[38] Murayama T, Takeuchi Y, Yamawaki K, Natsume T, Li M, Marcela RCN, *et al*. MCM10 compensates for Myc-induced DNA replication stress in breast cancer stem-like cells. Cancer Science. 2021; 112: 1209–1224. https://doi.org/10.1111/cas.14776.

[39] Yang WD, Wang L. MCM10 facilitates the invaded/migrated potentials of breast cancer cells via Wnt/β-catenin signaling and is positively interlinked with poor prognosis in breast carcinoma. Journal of Biochemical and Molecular Toxicology. 2019; 33: e22330. https://doi.org/10.1002/jbt.22330.

[40] Cui F, Hu J, Ning S, Tan J, Tang H. Overexpression of MCM10 promotes cell proliferation and predicts poor prognosis in prostate cancer. The Prostate. 2018; 78: 1299–1310. https://doi.org/10.1002/pros.23703.

[41] Chen D, Zhong N, Guo Z, Ji Q, Dong Z, Zheng J, *et al*. MCM10, a potential diagnostic, immunological, and prognostic biomarker in pan-cancer. Scientific Reports. 2023; 13: 17701. https://doi.org/10.1038/s41598-023-44946-2.

[42] Abdel-Maksoud MA, Iqbal K, Gull S, Kumar SK, Mastoor M, Almutairi SM, *et al*. Immune modulation and prognostic significance of MCM10 in pan-cancer: a comprehensive analysis. American Journal of Translational Research. 2023; 15: 6451–6463.

[43] Wang Y, Chen H, Zhang J, Cheng ASL, Yu J, To KF, *et al*. MCM family in gastrointestinal cancer and other malignancies: From functional characterization to clinical implication. Biochimica et Biophysica Acta. Reviews on Cancer. 2020; 1874: 188415. https://doi.org/10.1016/j.bbcan.2020.188415.